sensors

MDPI

Article

A Convolutional Neural Network for Electrical Fault Recognition in Active Magnetic Bearings Systems

Giovanni Donati[1], Michele Basso[1], Graziano A. Manduzio[3], Marco Mugnaini[2], Tommaso Pecorella[1] and Chiara Camerota[1]

[1] Department of Information Engineering, University of Florence, Via di Santa Marta 3 50139 Florence, Italy; michele.basso@unifi.it (M.B.); giovanni.donati@unifi.it (G.D.); chiara.camerota@unifi.it (C.C.).
[2] Department of Information Engineering and Mathematics, University of Siena, Siena, Italy; marco.mugnaini@unisi.it.
[3] Department of Information Engineering, University of Pisa, Pisa, Italy; graziano.manduzio@unipi.it.

Abstract: Active magnetic bearings are complex mechatronic systems that consist of mechanical, electrical, and software parts, unlike classical rolling bearings. Given the complexity of this type of system, fault detection is a critical process. This paper presents a new and easy way to detect faults based on the use of a fault dictionary and Machine Learning. In particular, the dictionary was built starting from fault signatures consisting of images obtained from the signals available in the system. Subsequently, a convolutional neural network was trained to recognize such fault signature images. This work concentrates on recognizing the most frequent electrical faults that typically affect position sensors and actuators. This new method permits, in a computationally convenient way, that can be implemented in real time, to determine which component has failed and what kind of failure has occurred. Therefore, this fault identification system allows for determining, in the event of a fault, which countermeasure to adopt in order to enhance the reliability of the system. The performance of the proposed method is assessed by means of a case study concerning a real turbomachine supported by two active magnetic bearings for the oil and gas field. Seventeen fault classes have been considered and the neural network fault classifier reached an accuracy of 93% on the test dataset.

Keywords: Active Magnetic Bearing, AMB, Fault analysis, Convolutional Neural Networks, Fault dictionary, Rotordynamics.

1. Introduction

Active Magnetic Bearings (AMBs) are being increasingly used across a broad range of rotodynamic applications, ranging from small turbo molecular pumps for medical applications to large compressors in the megawatt range for the oil and gas field. Compared to classic contact bearings, AMBs offer several significant advantages. AMBs achieve a significant reduction in friction and in the associated wear by levitating the rotor relative to the stator parts. The elimination of friction also enables higher rotation speeds, greater system efficiency, and eliminates the need for cumbersome lubrication systems that are typically required for traditional bearings. Due to the inherently unstable nature of AMBs, a stabilizing feedback control is needed for proper functioning. Therefore, an AMB is a complex mechatronic system comprising various components, including the controller, position sensors and actuators. The synthesis of the controller is a critical aspect of AMB systems. Various controller structures and design processes can be used, as reviewed for example in [1] or in [2]. Among these, augmented PIDs are probably the most widespread choice in industry because of their versatility, accuracy, efficiency, and cost-effectiveness. All the controllers of AMB systems rely on precise measurements of the rotor position, for which a common choice is to use inductive or eddy current sensors, even if recently self-sensing sensors and optical sensors have also been introduced [3]. The effect of the choice of sensors is discussed for example here [4]. About the other components, PWM is

Citation: To be added by editorial staff during production.

Academic Editor: Firstname Lastname

Received: date
Revised: date
Accepted: date
Published: date

commonly used for driving the electromagnets that make the rotor levitate. The behavior of all the components in the loop contributes to determining the stiffness and damping of the bearings, that are directly related to the stability and performance of the closed-loop system. To improve the robustness of such a complex system, a fault detection and diagnostic system is advisable to ensure safe and reliable operation. As a result, several studies have developed methods to detect failures associated with the rotor or with the electrical and electronic components, as for example in [6] and in [7]. Failure detection in AMB system enables also to adopt safety strategies exploiting their closed loop architecture that can adapt to cope with the detected fault. In fact, due to their active nature, controllers can dynamically adjust the bearings behavior in real-time. Exploiting the power of internal information processing, an AMB system can enhance its survival chances and reliability. For this reason, fault tolerant AMB systems have been developed that can manage malfunctions, for example, using a reconfigurable control, as described in [6] or in [7].

For fault diagnosis systems, usually, the actual system behavior is compared to the expected one in nominal condition to identify a faulty system condition. Observers of the system, as described in [5], are typically used.

Another common approach for identifying faults is the simulation-before-test technique. It involves constructing a fault dictionary from simulations of a particular plant, which collects examples of fault signatures that can be used to train a classifier capable of recognizing different faults, as described for example in [8].

Traditionally, fault diagnosis has been based on analyzing signals in the time and frequency domains. However, this paper proposes an approach that exploits a fault dictionary made by images of signals in time-domain to train a simple convolutional neural network that has the goal to recognize the AMB system faulty conditions. Taking the available electrical signals as sources, generalized orbits are built and converted into discrete 2D images that are used to fill the fault dictionary, with a technique that generalizes and extends the approach proposed by Xunshi, who used the sensors signals to build orbits to detect mechanical failures [9]. A similar method is proposed by Jing et al., who in their paper proposed a feature-based learning and fault diagnosis method for gearbox condition monitoring [10]. The fault features were obtained by using a simulation tool, developed by some of the authors [11], capable of automatically building the entire fault dictionary, once the fault conditions are modeled. In the context of this work, only single electrical parametric faults have been considered for simplicity, but the fault classes can be extended including e.g. also mechanical faults as in [12].

To exploit the knowledge stored in the fault dictionary, this paper proposes a classifier based on a convolutional neural network (CNN), well-suited for image classification, [13, 14] trained with the fault signature examples. In the case of system fault, the trained convolutional neural network has the aim of identifying the faulty component and the type of fault that has occurred.

Compared to other methods proposed in the literature that rely on analyzing signals in the time domain, the proposed approach, losing the time dependence, offers a novel solution to detect and locate faults, making full use of the potential of smart systems like AMBs. Moreover, with the help of computationally efficient image processing and simple neural networks, this automatic online diagnostic system can be developed without excessive computational cost. Such systems could be exploited in advanced prognostic maintenance systems to enhance balance of plant capabilities over time as described in [15-17].

The paper structure is the following: Section 2 describes the AMB modeling adopted to build a simulation tool. Section 3 presents the developed fault dictionary by which a classifier can be trained. Section 4 describes the proposed model of image classifier. Section 5 presents a case study. Section 6 shows the case study results; conclusion follows.

2. System Modeling

3.1. AMB Background

An AMB, applied to a turbomachine, has the purpose of making the rotor levitate with respect to the stator. Normally, a turbomachine is equipped with at least five AMB control axes: four for the rotor radial dynamics (two per each radial bearing) and one for the axial one. Only the radial dynamics of the system has been considered since radial rotor dynamics are normally more complex than axial ones and for this reason has been chosen as object of this work. An AMB is composed of two opposed electromagnets that attract a ferromagnetic object, in this case the rotor, and try to maintain it in the center of the air gap. A radial bearing is composed of two AMB control axes that are able to attract the rotor in any direction in a plane. Figure 1 describes a classical cross section of a radial AMB bearing in a heteropolar configuration, as described in [2].

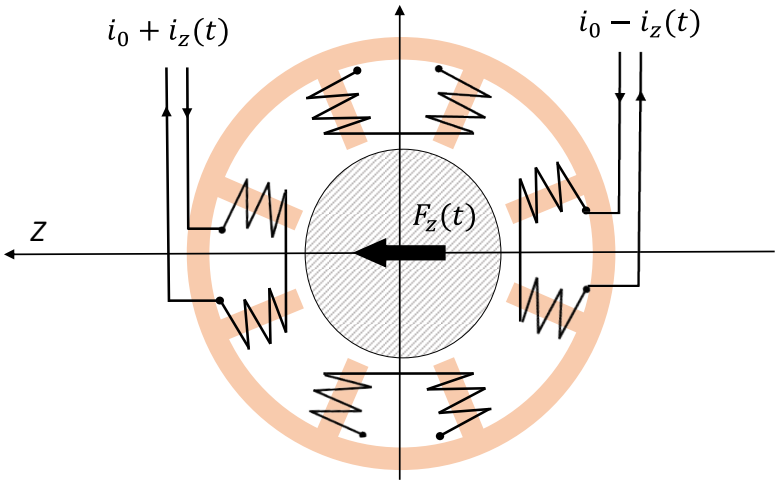

Figure 1. A classical cross section of a radial AMB in a heteropolar configuration.

The two opposed electromagnets are driven with a differential control current. Considering them, along an axis z, a linear relation can be found [18]:

$$F_z = k_i i_z - k_s Z \quad (1)$$

where F_z is the magnetic force exerted on the rotor along the axis z, Z is the displacement along the same axis with respect to the nominal working conditions and the parameters k_i and k_s respectively called electrical gain and negative stiffness depend on the geometrical parameters of the bearings and on the nominal operating conditions, that are the nominal air gap s_0 and the bias current i_0. Equation (1) is the more accurate the more the working conditions are close to the nominal ones. Because of the negative stiffness k_s, AMBs are inherently unstable. Hence, they are always inserted in a stabilizing closed loop system. Figure 2 shows a block diagram of an AMB system closed loop. This system comprises amplifiers for driving the magnetic bearings, position sensors comprising the related conditioning electronics, and a controller. The position sensors constantly monitor the rotor position, while the controller utilizes these signals to calculate the necessary control signals for the actuators, which drive the magnetic bearings. The goal of the closed loop system is to maintain the rotor in a levitated state at the center of the air gap by

determining the appropriate currents $\bar{\imath}$ for each AMB, where $\bar{\imath}$ is the control currents vector.

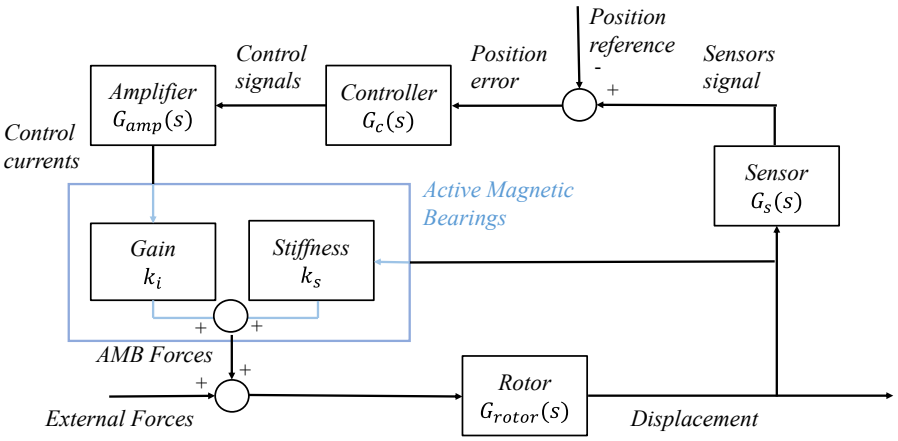

Figure 2. Block diagram of an AMB closed loop system.

3.1. AMB Closed Loop System Modeling

A state-space formulation was developed for each component to model the dynamics of the closed-loop system. The rotor radial state-space model was specifically constructed using a finite element method (FEM). This involved discretizing the rotor into N nodes along its geometric rotational axis. A Timoshenko modeling was utilized for the shafts, with a detailed description of the formulation available in [19] or [20]. The resulting equation that described the rotor dynamics is the following:

$$\begin{aligned} M\ddot{\bar{q}} + \left(C + \Omega C_g\right)\dot{\bar{q}} + (K - K_s)\bar{q} &= \bar{F}_{AMB} + \bar{F}_{ext} \\ \bar{F}_{AMB} &= K_i\bar{\imath} \end{aligned} \tag{2}$$

where M is the mass matrix, C is the damping matrix, C_g is the gyroscopic matrix, K is the stiffness matrix, Ω is the rotor rotational speed, $\bar{F}_{ext}$ are the external forces acting on the rotor, $\bar{F}_{AMB}$ are the AMB control forces, $\bar{q}$ is the vector that represents the position of every node of the rotor, $\bar{\imath}$ the vector of the control currents and, K_i and K_s respectively the matrix of current gains and the matrix of negative stiffnesses. Furthermore, a model order reduction technique was used on (2) to reduce the complexity of the system. In particular, modal truncation, described for example in [21], was used to eliminate all the rotor modes that are at a frequency above the range of interest for this type of application. Starting from (2), the rotor state space equation can be found:

$$\begin{aligned} \dot{\bar{X}}_R &= A_R\bar{X}_R + B_R(\bar{F}_{AMB} + \bar{F}_{ext}) \\ \bar{q} &= C_R\bar{X}_R \end{aligned} \tag{3}$$

where

$$\bar{X}_R = \begin{bmatrix} \bar{q} \\ \dot{\bar{q}} \end{bmatrix}, \quad A_R = \begin{bmatrix} [0] & I \\ -M^{-1}(K - K_s) & -M^{-1}\left(C + \Omega C_g\right) \end{bmatrix},$$

$$\mathrm{B_R} = \begin{bmatrix} [0] \\ M^{-1} \end{bmatrix}, \quad C_R = [I \quad [0]].$$

Moreover, linear state-space models were used to describe the other components of the AMB system, considering their unique characteristics and specifications. Combining the sensors, controller and actuators models, a second state-space system was found:

$$\begin{aligned}\dot{\bar{X}}_B &= A_B\bar{X}_B + B_B\bar{q}\\ \bar{F}_{AMB} &= C_B\bar{X}_B\end{aligned} \tag{4}$$

where $\bar{X}_B$ is the state and (A_B, B_B, C_B) are the matrices of the second state space model. Combining the equations (4) and (5), the state space model of the whole closed loop system was found:

$$\frac{d}{dt}\begin{bmatrix}\bar{X}_R\\ \bar{X}_B\end{bmatrix} = \begin{bmatrix}A_R & B_RC_B\\ B_BC_R & A_B\end{bmatrix}\begin{bmatrix}\bar{X}_R\\ \bar{X}_B\end{bmatrix} + \begin{bmatrix}B_R\\ [0]\end{bmatrix}\bar{F}_{ext} \tag{5}$$

The modeling of the whole system allows for simulating the dynamic behavior of the whole system. The main contributions of the term $\bar{F}_{ext}$ are the unbalance forces. Unbalance forces are synchronous forces with the speed of the rotor that are induced by the presence of unbalanced masses with respect to the axis of rotation of the rotor. The unbalance masses are due to inevitable manufacturing errors or rotor wear, and they are characteristic of a particular turbomachine. For a given axis x, at a fixed rotor speed Ω the unbalance force assumes the form:

$$F_{un_x} = \Omega^2 U\cos(\Omega t + \phi), \tag{6}$$

where ϕ is the phase of the unbalance respect other axis and U is the unbalance magnitude in kgm. In order to exactly reproduce the dynamic model, the machine is experimental identified to accurately assess the unbalance and to fine tune the state-space model (3). Some identification methods for AMB systems can be found in [22] or in [23].

3. Fault Dictionary

Due to the mechatronic structure of an Active Magnetic Bearing (AMB) system, failures can manifest in various forms, they can be software, electrical, or mechanical. These faults can result in the high-speed rotor making contact with its housing, potentially compromising the safety of the entire plant. Although touch-down bearings are designed to prevent direct contact between the rotor and housing, such an event must be avoided at all costs. To address the diverse range of faults that can arise in AMB systems, several measures can be taken, including redundancies, quality control, individual measures, and various control strategies. Active fault diagnostics and corrections can also be employed. Guidelines for designing a reliable system are provided in ISO 14839 [24] and API 617 [25] for turbomachinery on AMBs in the oil and gas field. A three-stage process for dealing with faults is described in [26], which involves determining the timing of the fault, identifying the faulty component, and identifying the type of fault. Given the complexity of the system, there are numerous reasons why malfunctions can occur, which can have different degrees of impact on system performance. [27] summarizes the main causes of malfunctions, their occurrence, and severity. This work takes into consideration the most common electrical soft faults, which can be modeled in three different ways: multiplicative, bias, and noise, as discussed in [28]. More specifically, this work considered the most frequent scenario, i.e., that of a single fault at a time. Figure 3 provides a summary of these faults.

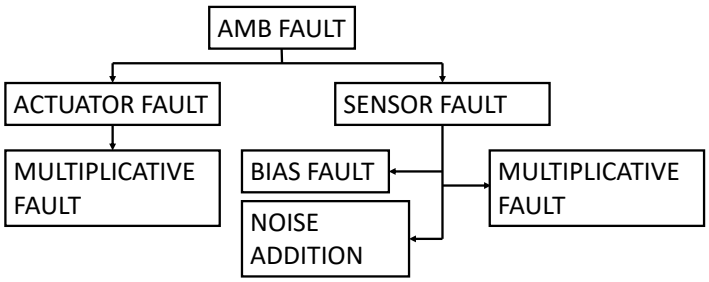

Figure 3. Resume of common electrical faults of AMB system

Steady-state signals, obtained from sensors and control systems are exploited to build images that serve as fault signatures. In particular, in this work the available considered signals were position signals from sensors, control signals from the controller, and current signals from the actuators, that are generally easily obtainable in an AMB system. Figure 4 summarizes the electrical signals that were chosen to build the dictionary. Since all signals exhibit periodic behavior, during normal machine operations at a constant fixed rotational speed, it is possible to create groups of images by representing the signals related to one of the two orthogonal control axes as functions of those related to the other axis, disregarding time as an independent variable and obtaining generalized orbits of the signals related to each bearing, as described in Figure 4.

The fault features were obtained by using a simulation tool capable of automatically building the entire fault dictionary once the fault conditions are modeled. The simulation tool is implemented in the Matlab-Simulink environment and allows for performing Monte Carlo simulations, by varying a selected set of component parameters using specific probability distributions or by adding noisy signals. The developed simulation tool was validated by comparing the results obtained with a commercial software (MADYN 2000).

Reference images, relative to non-faulty condition, are formed by simulating machine operations at a constant rotor speed and collecting signals while varying the component parameters within their tolerance ranges and accounting for normal levels of noise. The dictionary is completed by simulating the different faults that belong to the previously introduced fault classes. In detail, examples of each single soft fault signatures in the fault classes listed above, are obtained by randomly varying all the electrical parameters (gains, sensitivity and biases) within the tolerance ranges, but for the faulty component which varies outside this range, or by injecting noise with an abnormal standard deviation.

The variations of the component parameters in the tolerance ranges determine regions of confidence in the reference images relative to non-faulty condition where the generalized orbits should remain under fault-free conditions. If the orbits go beyond these regions, a fault has occurred. The built fault dictionary consists of images containing the deformed orbits with respect to the reference ones, given by simulating the different faults for the particular plant.

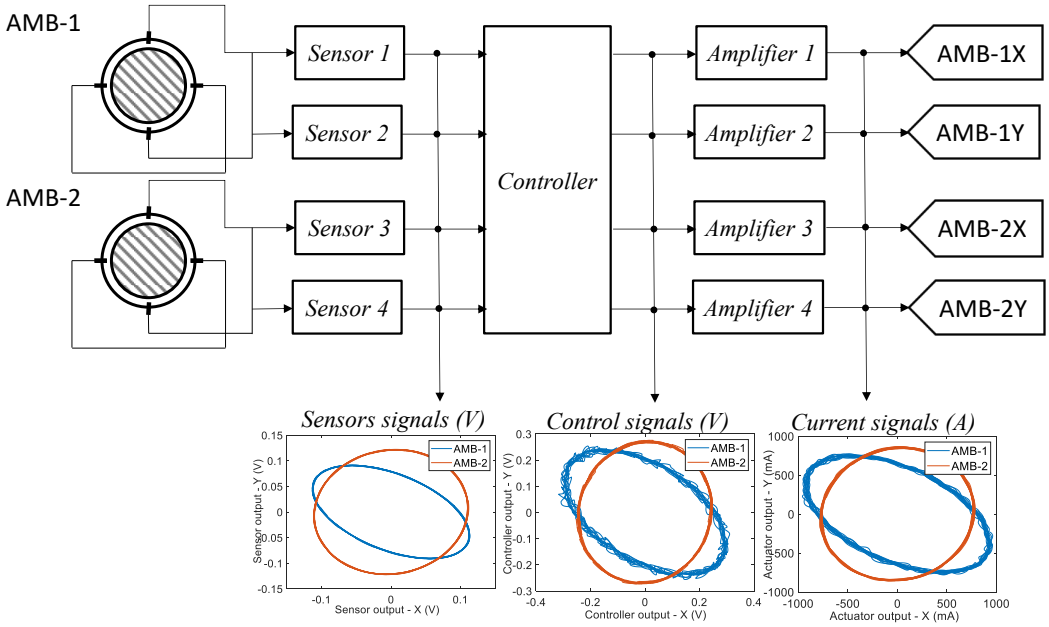

Figure 4. Summary of electrical signals that were chosen to build the dictionary.

Once the simulations are done, the feature images can be built. The time signals were normalized, and the orbits triplets were represented by images with a fixed resolution. Black and white images were generated through the Matplotlib library in Python, one for each orbit typology, one for the control signals, one for the position signals and the last for current signals. In the end, these images were concatenated into a unique RGB image, so that each RGB channel concerns only one orbit typology. In other words, for every triplet of images, related to a particular scenario, a unique RGB color was associated at each orbit typology, the red for the position signals, the blue for control signals and the green for current signals. Directly using images from available signals to train the classifier improves the ability of the system to understand the AMB system state, which offers a wider view and enhances the precision of information captured.

4. Classification Algorithm: Convolutional Neural Network

The proposed classifier exploits a Convolutional Neural Network (CNN), a neural network specialized for processing data that has a known, grid-like topology [29]. Examples include time-series data, which can be thought of as a 1D grid, and image data, which are 2D grid of pixels. LeCun et al [30] first applied the backpropagation algorithm to CNNs, with LeNet, a network developed to recognize handwritten digits. AlexNet [31] became the first modern deep convolutional neural network, representing a breakthrough in image classification.

A CNN is an architecture composed of multiple layers that collaborate to process and extract meaningful features from input data, each of them acting a different function in the network operations.

Convolutional layers consist of multiple filters, or kernels, that slide over the input data and perform convolutions. Each filter extracts specific features by detecting patterns and spatial information. The output of each filter is a feature map. An activation function, which introduces non-linearity into the network, is usually applied after each convolutional layer. Common choices include Rectified Linear Unit (ReLU), or variants such as Leaky ReLU or Parametric ReLU.

Pooling layers are frequently used after the convolutional layers to reduce the dimensionality of the feature maps and spatial dimensions. This down-sampling process helps

summarize and extract the most important information from the feature maps while reducing the network's computational complexity. In other words, max pooling is a commonly used technique in which the maximum value within a pooling window is selected as the representative value for that region.

After the convolutional and pooling layers, the feature maps are flattened into a one-dimensional vector. This vector is then fed into fully connected layers, also called dense layers, which are responsible for making predictions or classifications based on the extracted features. Like convolutional layers, activation functions are applied in the fully connected layer to introduce non-linearity.

Finally, the last layer of CNNs is the output layer, which computes the network predictions. This time, the activation function used depends on the type of problem being solved. For classification tasks, as for this work, Softmax activation is commonly used to generate a probability distribution over the classes [32].

A loss function is used to measure the discrepancy between the predicted outputs and the ground truth labels. The choice of loss function depends on the problem type, such as categorical cross-entropy for multi-class classification, as in the proposed model [33].

During training, the parameters of the CNN are adjusted to minimize the loss function using optimization algorithms like stochastic gradient descent (SGD) or its variants, such as Adam Optimizer [34]. This process, known as backpropagation, updates the weights and biases of the network to improve its performance. The structure of a CNN, depicted in Figure 5, is very complex; however, many modern machine learning frameworks, like PyTorch, implement the above-described CNN operation.

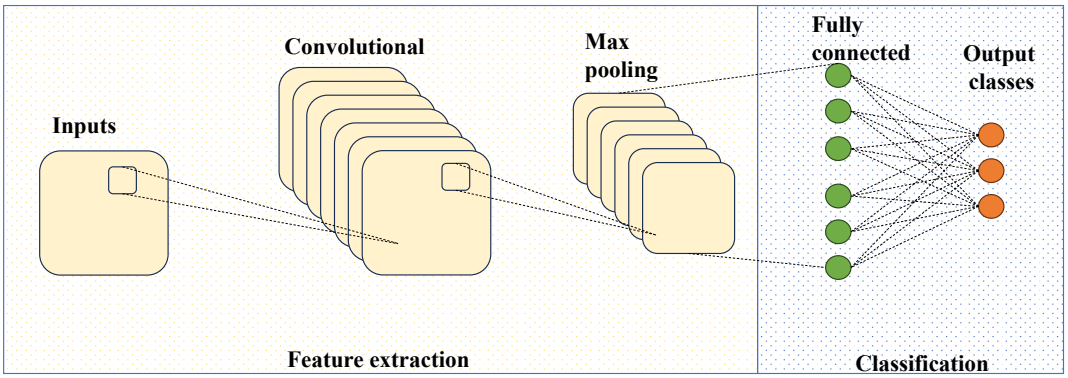

Figure 5. Schematic structure of CNN.

4.1 Proposed model

In this work, the CNN classifier has the final objective of recognizing 17 fault classes, among which 16 are fault classes and 1 is the nominal class related to the normal operation condition. These classes are summarized in Figure 6 and refer to Figure 3.

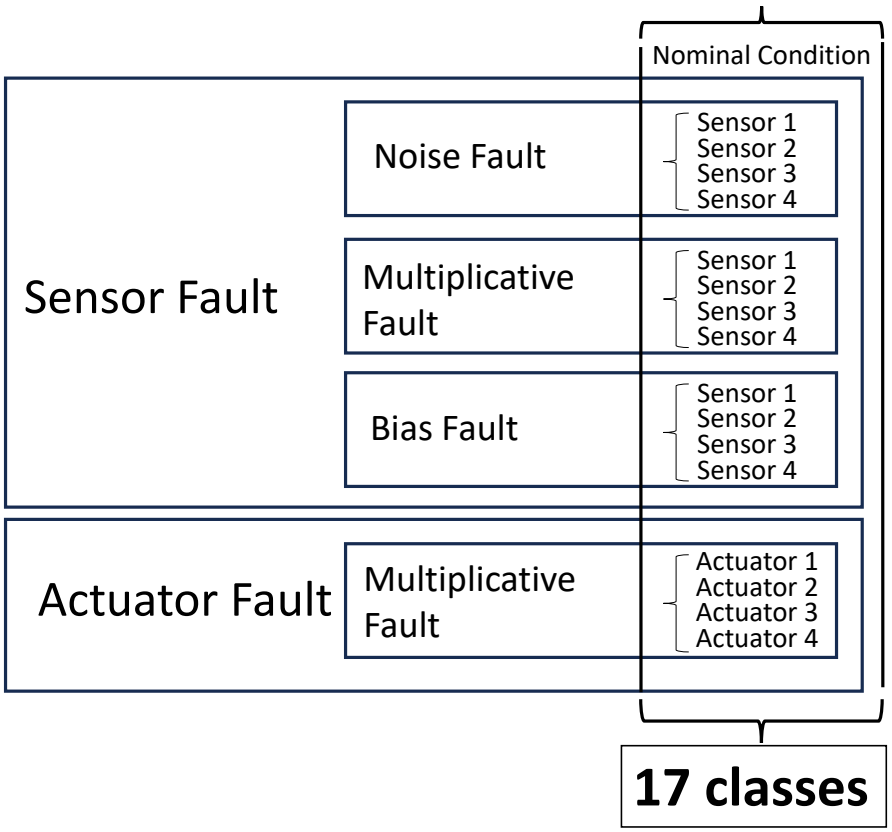

Figure 6. Summary of the classes to be classified.

The proposed CNN model consists of a series of alternately stacked convolutional, pooling and fully connected layers, as shown in Figure 7.

It employs convolutional layers to extract features, max pooling to down-sample the feature maps, and fully connected layers to map the extracted features to the output classes.

The first layer was a convolutional 2D, which has the images of orbit triplets as input channels while the output channels were the 17 classes described in Table 1. In this way, the layer was able to expand the information of the provided data. With the same purpose, a second convolutional layer was implemented. Then, a max pooling was computed, halving the dimensions of the images both for considering the expanded information and for preventing the gradient explosion. At this point, another convolutional 2D layer increased the dimension again, from 16 to 36 followed by another max pooling, for the same reasons explained above.

Subsequently, a batch normalization layer was applied to the extracted features in the previous layers. This layer allows for using high learning rates and is quite unaffected by initialization. Moreover, it eliminates the need for dropout since it performs a regularization on the parameters, as explained in [35].

Afterwards, two additional convolutional layers were introduced. Unlike the preceding layers, these new layers aimed to combine or "zip" the output from the previous layer, thereby extracting the most significant features. This process helps to enhance the representation of the data by capturing more complex patterns and relationships.

The convolutional part of the network was concluded with a final max pooling operation. This step was followed by the transition to a fully connected layer. To prepare the data for

this transition, the three-dimensional tensor resulting from the previous layers was flattened into a one-dimensional vector. Subsequently, three linear layers were trained in the network. Each of these layers was responsible for transforming the data and adjusting its dimensions to align with the output classes. In this case, the output dimension of each linear layer was rounded off to 17, which matches the number of classes in the classification task.

In the proposed model, each convolutional layer has a kernel dimension of 3x3 and a step dimension of 1x1, while the max pooling layers have a step dimension of 2x2. At least, each convolutional and fully connected layer, except the last one, was adhered with a ReLu activation function. Adam optimizer was used, which is computationally efficient, has low memory requirements, is invariant to diagonal rescaling of gradients, and is well suited to problems with large data and/or parameters [34]. The architecture was implemented using the PyTorch libraries.

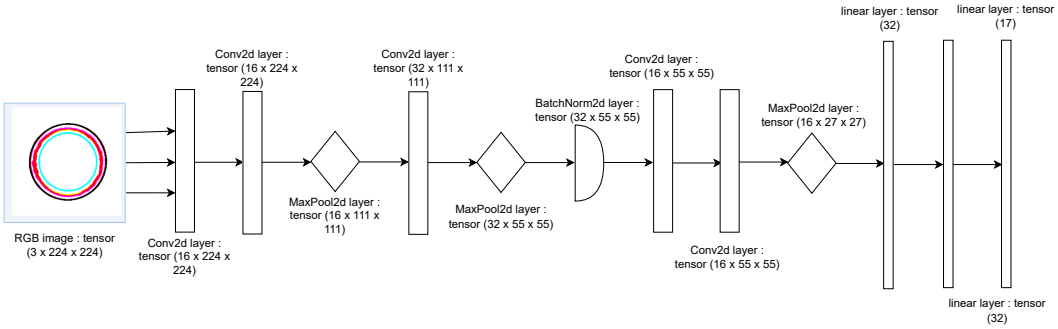

Figure 7. The proposed model structure.

5. Case Study

As a case study to assess the performance of the proposed diagnosis system an AMB supported system was considered. The case study is a real medium-size compressor supported by AMBs for the oil and gas field. Figure 8 illustrates the finite element model of the rotor under investigation with a mass of about 810 kg and a length of about 1.80 meters. Regarding the electrical part, the controller structure was an augmented PID. It has a decentralized structure, that divides the system into control axes and every control axis is controlled independently. For what concerns the other components, the system comprises switching pulse width modulation (PWM) amplifiers with heteropolar AMB actuators and inductive position sensors with a band of 4 kHz.

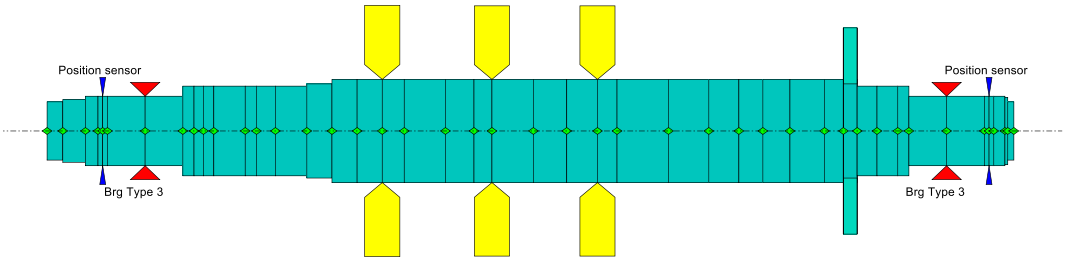

Figure 8. This image shows the finite element model of the rotor, where the red triangles are the bearings, the yellow elements are the disks, and the blue elements are the sensors.

Under nominal conditions, the system features a constant rotor rotation speed of 7800 rpm and an unbalance of $2.10 \times 10^{-3}\ kg \times m$ positioned at the center of mass of the rotor. The fault free condition is given by variations of the sensor sensitivities within a 2% tolerance

of sensor, bias below 1 µm, and in the presence of a Gaussian white noise with a standard deviation of 1 µm. As for the actuators, a 2% tolerance of the DC gain is taken into consideration. Figure 9 displays an example of nominal condition orbits related to the fault-free signatures for the two radial bearings of the rotor.

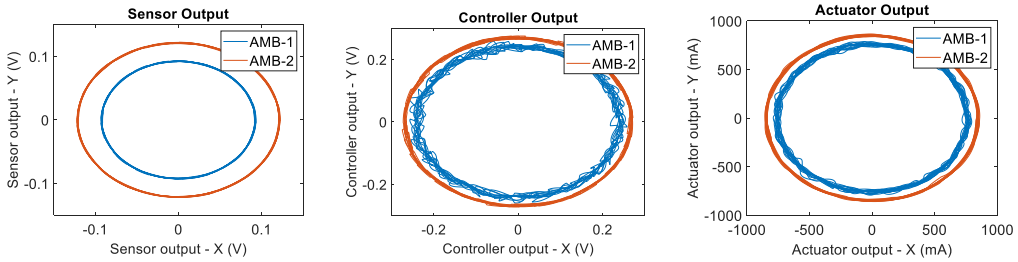

Figure 9. This image shows an example of nominal condition orbits. On the left the sensor output, in the center the controller output and on the right the actuator output are reported.

The faulty conditions that were taken into account to form the classes of the fault dictionary were computed through Monte Carlo analysis using specific parameter distribution. In particular, for each actuator multiplicative fault, the faulty actuator gain was chosen as a uniformly distributed random number out of the tolerance range centered in the nominal value in an interval ±50% the nominal value. Similarly, for each sensor multiplicative fault, the faulty sensor gain was chosen as a uniformly distributed random number out of the tolerance range centered in the nominal value in an interval ±50% of the nominal value. Instead, for each sensor noise fault, the faulty sensor is subjected to a gaussian additive noise with a standard deviation up to five times the nominal level of noise. Finally, for each sensor bias fault, the faulty sensor has random bias amplitude larger up to five times the nominal level of bias. Figure 10 shows an example of how orbits change shape when a specific fault occurs with respect to the orbits related to the nominal conditions reported for example in Figure 9.

The dataset used in the case study consists of 37600 RGB images obtained from different simulations, as described above in Section 3. More specifically, each image has a size of 3×224×224, where 3 represents the RGB channels and 224 x 224 is the number of pixels used for each image. Figure 11 gives an example of the used RGB images. The dataset is composed of 5600 examples of the fault free condition and 2000 examples of all the other 16 fault classes.

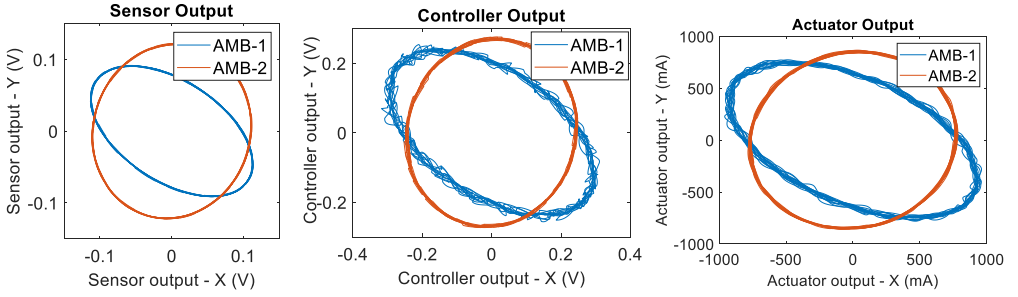

Figure 10. Example of signals orbits related to a sensor multiplicative fault, in particular, an AMB-1 x-axis multiplicative fault of -50% with respect to the nominal value.

Before training, data were pre-processed with aim of enhancing the model performance in terms of accuracy while also reducing noise interference. The dataset was divided into a training set, which includes 90% of the examples, and a test and a validation set, each which collects 5 % of the remaining examples.

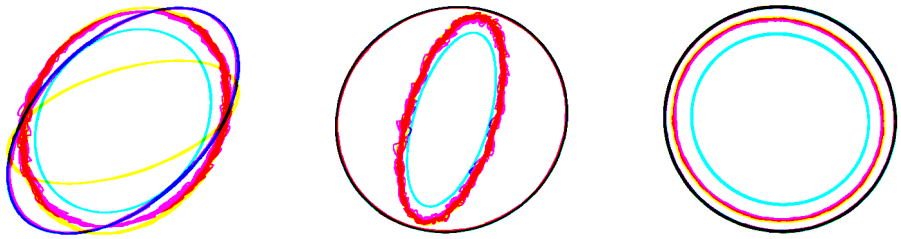

Figure 11. The RGB images used for training. In the right and central panel are shown, respectively, actuator and sensor gain fault. In the panel of left, nominal condition is shown.

6. Results and Discussion

The model was trained using the pre-processed training set for a total of 1000 epochs. Using the test set, the proposed CNN was validated, in fact, the reached test set accuracy was of about 93 %, while the training set accuracy reached was about 95 %. These results are presented in Figure 12, with the test set accuracy depicted in orange and the training set performance in pink.

Figure 13 shows the test and accuracy ratio, it represents the ratio between the accuracy of train and test reported in Figure 12. The descending trend observed in this plot suggests that the CNN's estimated parameters are not affected by overfitting. This indicates that the model has achieved a good level of generalization, meaning it can effectively generalize its learned patterns and make accurate predictions on unseen data.

Additionally, in Figure 14, the obtained confusion matrix is reported, and Table 1 presents the codebook of the labels. The horizontal axis of the matrix represents the actual faults, while the vertical axis represents the predicted faults. The diagonal elements show the percentage of correct predictions, the values above the diagonal indicate false positives, while the lower ones represent false negatives.

As shown by Figure 14, the confusion matrix is quite diagonal even though the lowest values are about 70 %.

It was found that the most part of misclassifications are related to soft faults related to small parametric deviations (with respect to the fault-free condition).

The achieved accuracy is really satisfactory for soft fault recognition taking into account also small parametric variations. This fact was due to two reasons. The first is that the regions of parameters variation related to faults border on the tolerance regions. The second reason is that the image resolution is limited. These facts lead some classes not to be recognized correctly, more precisely, the faulty class that are related to orbits that differ of a small amount with respect the reference ones in presence of small variation of a parameter out of the tolerance. This is a problem intrinsic in the definition of soft fault itself. No net borders between the faulty and the fault free condition exist, but in any case, positive or negative false related to these borderline situations have no severe consequences.

{IMG}

Figure 12. On the left plot the training accuracy for each epoch is shown, on the right the testing accuracy for each epoch is reported.

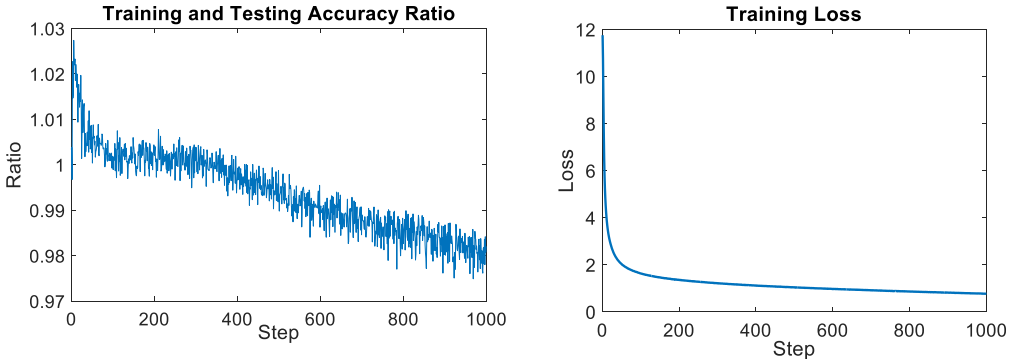

Figure 13. On the left the training and testing accuracy ratio plot is shown and on the right the training loss plot is reported.

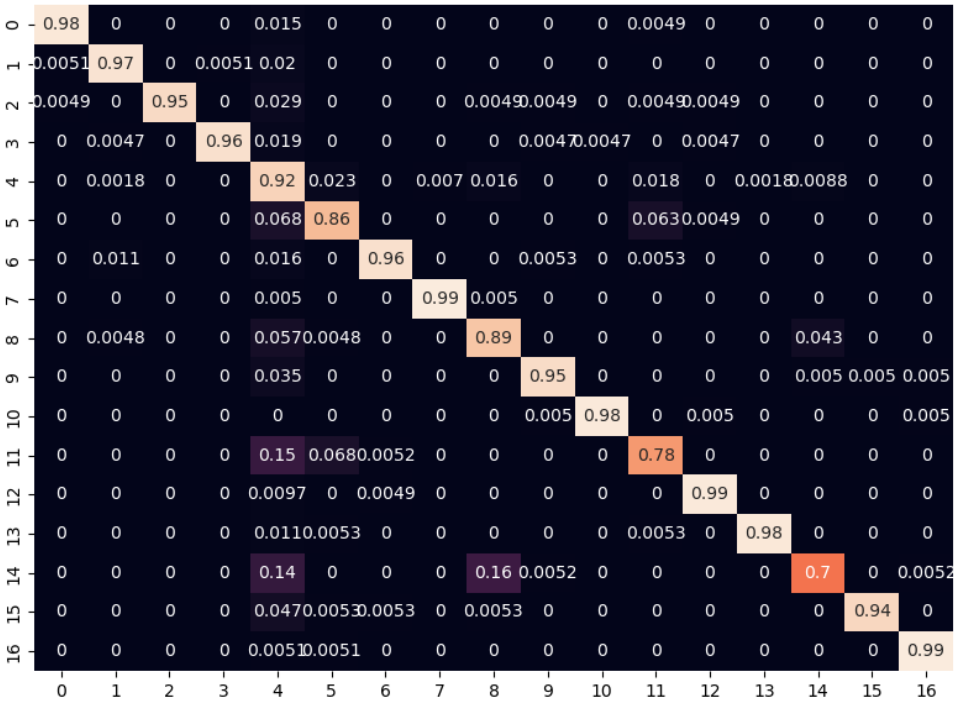

Figure 14. Obtained confusion matrix.

ID	Component	Kind of fault	ID	Component	Kind of fault
0	Actuator 1	Gain Fault	9	Sensor 2	Gain Fault
1	Actuator 2	Gain Fault	10	Sensor 2	Noise Fault
2	Actuator 3	Gain Fault	11	Sensor 3	Noise Fault
3	Actuator 4	Gain Fault	12	Sensor 3	Gain Fault
4	-	Nominal Condition	13	Sensor 3	Noise Fault
5	Sensor 1	Bias Fault	14	Sensor 4	Bias Fault
6	Sensor 1	Gain Fault	15	Sensor 4	Gain Fault
7	Sensor 1	Noise Fault	16	Sensor 4	Noise Fault
8	Sensor 2	Bias Fault			

Table 1. Codebook of the confusion matrix.

6. Conclusion

Active Magnetic Bearings are gaining popularity in a range of rotating machinery applications due to their high performance and the elimination of cumbersome lubrication systems. On the other hand, they require a complex closed-loop mechatronic system to operate. Therefore, to ensure safe and reliable operation, fault detection and diagnostic systems are necessary. This proposed novel approach for fault diagnosis utilizes images of electrical signals available in an AMB system to train a classifier: a simple convolutional neural network that was trained to detect the most common soft electrical faults. Remarkably, the proposed classifier exhibits high accuracy and generalizability without requiring an extensive amount of data. This approach can be easily extended to other fault typologies and to other AMB-supported systems.

Acknowledgments: Baker Hughes Company supported this study in part.

Conflicts of Interest: The authors declare no conflict of interest.

References

1. Srinivas R. Siva, Tiwari R., Kannababu Ch. Application of active magnetic bearings in flexible rotordynamic systems–A state-of-the-art review. *Mechanical Systems and Signal Processing*, **2018**, 106, 537-572.
2. Bleuler H., Cole M., Keogh P., Larsonneur R., Maslen E., Okada Y., Schweitzer G., A. Traxler. *Magnetic bearings: theory, design, and application to rotating machinery*. Springer Science & Business Media, 2009.
3. Tantau Mathias, Morantz Paul, Shore Paul. Position sensor for active magnetic bearing with commercial linear optical encoders. *CIRP Annals*, **2021**, 70.1, 419-422.
4. M. Basso, G. Donati and M. Mugnaini. A simulation tool for sensor selection in AMB rotor supported systems. In Proceedings of 2023 IEEE International Instrumentation and Measurement Technology Conference (I2MTC), Kuala Lumpur, Malaysia, 2023.
5. Da Silva, Gilberto Machado, Pederiva Robson. Fault diagnosis of active magnetic bearings. *Mechatronics*, **2022**, 84, 102801.
6. Sarmah Nilakshi, Tiwari Rajiv. Analysis and identification of the additive and multiplicative fault parameters in a cracked-bowed-unbalanced rotor system integrated with an auxiliary active magnetic bearing. *Mechanism and Machine Theory*, **2020**, 146, 103744.
7. Tsai Nan-Chyuan, King Yueh-Hsun, Lee Rong-Mao. Fault diagnosis for magnetic bearing systems. *Mechanical systems and signal Processing*, **2009**, 23.4, 1339-1351.
8. Caciotta M., Cerqua V., Leccese F., Giarnetti S., De Francesco E., De Francesco E.; Scaldarella N. A first study on prognostic system for electric engines based on Envelope Analysis. In Proceedings of 2014 IEEE Metrology for Aerospace (MetroAeroSpace), Benevento, Italy, 2014, 362-366.
9. Yan X., Zhang C. A., Liu Y. Multi-branch convolutional neural network with generalized shaft orbit for fault diagnosis of active magnetic bearing-rotor system. *Measurement*, **2021**, 171, 108778.
10. Jing L., Zhao M., Li P., Xu X. A convolutional neural network-based feature learning and fault diagnosis method for the condition monitoring of gearbox. *Measurement*, **2017**, 111, 1–10.
11. M. Basso, G. Donati and M. Mugnaini. Smart Fault Dictionary for Active Magnetic Bearings Systems. In Proceedings of International Workshop on Metrology for Industry 4.0&IoT (MetroInd4.0&IoT), Brescia, Italy, 2023.
12. Yan X., Sun Z., Zhao J., Shi Z., Zhang C. A. Fault diagnosis of active magnetic bearing–rotor system via vibration images. *Sensors*, **2019**, 19.2, 244.
13. Ciregan D., Meier U., Schmidhuber J., Schmidhuber Jürgen. Multi-column deep neural networks for image classification. In Proceedings of 2012 IEEE conference on computer vision and pattern recognition. IEEE, 2012, 3642-3649.
14. Ajit A., Acharya K., Samanta A. A review of convolutional neural networks. In Proceedings of 2020 international conference on emerging trends in information technology and engineering (ic-ETITE) IEEE, 2020, 1-5.
15. Fort A., Bertocci F., Mugnaini M., Vignoli, V., Gaggii V., Galasso A., Pieralli M. Availability modeling of a safe communication system for rolling stock applications. In Conference Record - IEEE Instrumentation and Measurement Technology Conference, 2013, pp. 427–430, 6555453.
16. Ceschini G., Mugnaini M., Masi A. A reliability study for a submarine compression application. *Microelectronics Reliability*, **2002**, 42(9-11), pp. 1377–1380.

17. Catelani M., Ciani L., Mugnaini M., Scarano V., Singuaroli R. Definition of safety levels and performances of safety: Applications for an electronic equipment used on rolling stock. In 2007 IEEE Instrumentation & Measurement Technology Conference IMTC 2007 (pp. 1-4).
18. Swanson E. E., Maslen E. H., Li G, Cloud C. H. Rotordynamic design audits of AMB supported machinery. In Proceedings of the 37th Turbomachinery Symposium. Texas A&M University. Turbomachinery Laboratories, 2008.
19. Lalanne M., Ferraris, G. *Rotordynamics prediction in engineering*. Wiley, 1998.
20. Friswell M. I., Penny J. E., Garvey S. D., Lees A. W. *Dynamics of rotating machines*. Cambridge university press, 2010.
21. Z. Gosiewski, Z. Kulesza. Virtual collocation of sensors and actuators for a flexible rotor supported by active magnetic bearings. In Proceedings of the 14th International Carpathian Control Conference (ICCC), Rytro, Poland, 2013, 94-99.
22. Aenis M., Knopf E., Nordmann R. Active magnetic bearings for the identification and fault diagnosis in turbomachinery. *Mechatronics*, **2002**, 12.8, 1011-1021.
23. Sun Z., He Y., Zhao J., Shi Z., Zhao L., Yu S. Identification of active magnetic bearing system with a flexible rotor. *Mechanical Systems and Signal Processing*, **2014**, 49.1-2, 302-316.
24. ISO 14839-3:2006 Mechanical vibration — Vibration of rotating machinery equipped with active magnetic bearings — Part 3: Evaluation of stability margin.
25. API Standard 617. Axial and centrifugal compressors and expander-compressors for petroeluem, chemical and gas industry services. Eight edition, American Petroleum Institute, Washington D.C, **2014**.
26. Frank Paul M., Ding Steven X., Marcu Teodor. Model-based fault diagnosis in technical processes. *Transactions of the Institute of Measurement and Control*, **2000**, 22.1, 57-101.
27. Lijesh K. P., Hirani H. Failure Mode and Effect Analysis of Active Magnetic Bearings. *Tribology in Industry*, **2016**, 38.1.
28. Kim Seung-Jong, Lee Chong-Won. Diagnosis of sensor faults in active magnetic bearing system equipped with built-in force transducers. *IEEE/ASME transactions on mechatronics*, **1999**, 4.2, 180-186.
29. I. Goodfellow, Y. Bengio, A. Courville. *Deep learning*. The MIT Press, 2016.
30. Y. Lecun, L. Bottou, Y. Bengio, P. Haffner. Gradient-based learning applied to document recognition. In Proceedings of the IEEE, vol. 86, no. 11, 2278-2324, Nov. 1998.
31. Krizhevsky Alex, Ilya Sutskever, Geoffrey E. Hinton. Imagenet classification with deep convolutional neural networks. *Communications of the ACM,* 60.6, **2017**, 84-90.
32. Liu W., Wen Y., Yu Z., Yang M. Large margin softmax loss for convolutional neural networks. *arXiv preprint arXiv*, **2016**, *1612.02295*.
33. Zhang Z., Sabuncu M. Generalized cross entropy loss for training deep neural networks with noisy labels. *Advances in neural information processing systems*, **2018**, 31.
34. Kingma D. P., Ba J. Adam: A Method for Stochastic Optimization. *ArXiv. /abs/1412.698*, **2014**.
35. Ioffe S., Szegedy C. Batch Normalization: Accelerating Deep Network Training by Reducing Internal Covariate Shift. *ArXiv. /abs/1502.03167*, **2015**.